APPLICATION OF TITANIUM CARBIDE FILMS FOR SWEAT COMPONENTS MONITORING

MARIYA ALEKSANDROVA[1*], RADE TOMOV[1], VELICHKA STRIJKOVA[2] AND VESELA KATROVA[2]

[1]*Department of Microelectronics, Faculty of Electronic Engineering and Technologies Technical University of Sofia 8 Kliment Ohridski blvd., 1000 Sofia, Bulgaria*
e-mail: m_aleksandrova@tu-sofia.bg

[2]*Institute of Optical Materials and Technologies "Acad. Yordan Malinovski", Bulgarian Academy of Sciences, 1113 Sofia, Bulgaria*

Abstract. In this study, a water-based eco-friendly solution of Titanium Carbide MXene was ultrasonically spray-coated on a Si/SiO_2 substrate for the detection of sweat substances. The optimal flow rate of the solution was found to be 0.15 ml/min, and the optimal substrate temperature was 130 ºC. The resulting films had a surface roughness of ~ 17 nm. Chemoresistive sensors with titanium and aluminum contacts were fabricated, and their response to some sweat components, such as $MgCl_2$, NH_3, and NaCl, was measured. The most stable and strongest response was toward $MgCl_2$ measured from the sensors with Ti contact. The response and recovery times of chemoresistive sensors based on MXene/Ti interface were determined to be in the range 20-60 s for the $MgCl_2$ concentration in the range 10-40 mg/mL (typically existing in the human sweat) and 30-100 s for the NH_3 concentrations in the range 0.5-2 mg/mL. These measurements can be practically useful as indicators for proper electrolyte balance and hydration status, which can be correlated to health implications.

Keywords: ultrasonic deposition; titanium carbide films; electrical interfaces; biosensors.

1. INTRODUCTION

The assessment of human physiological condition through the analysis of biochemical compounds present in bodily fluids and excretions - namely saliva, exhaled breath, and perspiration (sweat) - has emerged as a significant area of investigation due to its non-invasive nature, offering potential for early detection of developing

*Corresponding author
http://doi.org/10.7546/EngSci.LXII.25.04.01

pathologies and identification of previously unnoticed health concerns. This approach contrasts sharply with traditional diagnostic methods that often require invasive procedures, such as blood draws or biopsies, which can be uncomfortable, carry risks, and are less amenable to frequent or continuous monitoring.

Specifically, the aforementioned biochemical compounds function as biomarkers, serving as measurable indicators of specific physiological states or pathological conditions. The presence and concentration of these molecules provide a snapshot of the body's internal environment, reflecting the interplay of various metabolic processes and system functions. Alterations in the normal physiology of a human organism, stemming from disease processes or other disturbances, are often mirrored by detectable shifts in the concentrations of specific molecules found in saliva, breath, or sweat. These changes can serve as early warning signs, prompting further investigation and potentially enabling timely intervention.

A diverse mix of compounds is secreted within sweat, and fluctuations observed in their respective concentrations can signal underlying disruptions in human health, including conditions such as hepatic dysfunction (liver disease), oncological processes (cancer), metabolic disorders like diabetes mellitus, and even neurodegenerative ailments like Parkinson's disease [1]. For instance, elevated levels of certain proteins or metabolites in sweat might indicate liver damage or the presence of cancerous cells, while imbalances in glucose or insulin-related compounds could point to diabetic complications. Furthermore, the monitoring of ionic concentrations in sweat, with specific regard to ions such as sodium (Na^+), magnesium (Mg^{2+}), and chloride (Cl^-), and their compounds, is of critical importance. These ions play vital roles in maintaining fluid balance, nerve impulse transmission, and muscle contraction. Deviations from normal concentrations can provide clues to conditions like dehydration, a state of inadequate bodily fluid volume, and the genetic disorder cystic fibrosis [2]. Cystic fibrosis, characterized by impaired chloride transport across cell membranes, results in abnormally high chloride levels in sweat, forming the basis of a diagnostic test. Tracking mineral losses through perspiration is also essential to ensure the maintenance of proper electrolyte balance, crucial for optimal physiological function [3]. Significant electrolyte depletion, especially during strenuous activity or in hot environments, can lead to muscle cramps, fatigue, and more severe complications.

In the pursuit of advanced sensing technologies for sweat analysis, various nanomaterials are under intense investigation for integration into sensing structures. Nanomaterials, possessing unique physical and chemical properties due to their size and composition, offer the potential for highly sensitive and selective detection of target biomarkers. These materials include carbon nanotubes, graphene, metallic nanoparticles, metal-oxide nanoparticles, and polymeric materials [4]. These nanomaterials are frequently employed in chemoresistive sensor designs, wherein a change in the electrical resistance of the sensing element occurs in response to chemical interactions with the target analytes [5]. Chemoresistive sensors rely on the principle that

the adsorption or binding of specific molecules to the sensing material alters its electronic structure, leading to a measurable change in resistance. The sensitivity of these sensors can vary depending on the target molecule, and this variance is primarily governed by the adsorption energy, which refers to the strength of interaction between the analyte molecule and the sensing material, and the charge transfer mechanism, which describes the movement of electrons between the analyte and the sensing material, ultimately dictating the sensor's selectivity and responsiveness [6]. The higher the adsorption energy and the more efficient the charge transfer, the greater the sensor's response to a particular analyte. This allows for the design of sensors that are specifically tuned to detect certain biomarkers with high precision.

Among the nanomaterials applicable as sensing layers within chemoresistive sensors for sweat analysis are MXenes, a class of two-dimensional materials gaining prominence in sensing applications. MXenes combine high electrical conductivity, large surface area, and tunable surface chemistry, making them ideally suited for chemoresistive sensing. MXenes are synthesized through the selective etching of the "A" element layer from a crystalline MAX phase precursor (illustrated in Fig. 1). The MAX phase is a ternary carbide or nitride with the general formula $M_{n+1}AX_n$, where *M* represents a transition metal, *A* is an element typically aluminum or silicon, and *X* is carbon or nitrogen [7]. During the etching process, the *"A"* layer is chemically removed, leaving behind the multi-layered MXene structure.

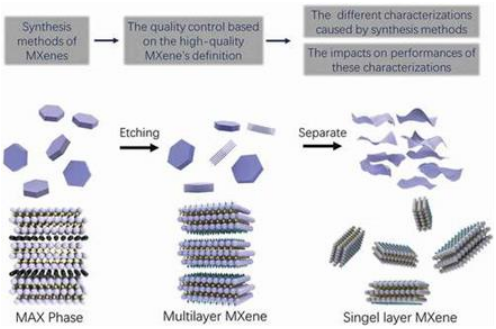

Fig. 1. Fabrication process of MXenes [8]

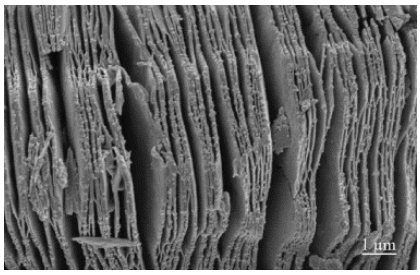

Fig. 2. Scanning electron microscopy (SEM) image of MXenes [9]

After the etching of the *A* elements, the resulting nano-sheets left behind form an accordion-like structure (Fig. 2). The advantages of the MXenes are tunable electrical conductivity and a high surface-to-volume ratio, which makes them very promising materials for selective chemoresistive sensors. One of the MXenes is titanium carbide – $Ti_3C_2T_x$, fabricated by etching the aluminum in the Ti_3AlC_2 MAX phase. T_x are surface functional groups, which are –O, -OH, -F [7] that also improve the potential for sensing applications, as they interact with the targeted molecules [10].

Considering the intended application of the sensor, whether for portable or wearable devices, the MXene film requires deposition onto an appropriate substrate, which

may be either a rigid, solid-state material or a flexible one. The diverse range of substrates exhibits varying surface wettability characteristics; consequently, some situations necessitate an additional pre-deposition treatment to optimize MXene film formation. Substrate wettability significantly affects the adhesion and uniformity of the deposited MXene layer. In consideration of the specific substrate attributes - including its thermal capacity, hydrophobic or hydrophilic nature, and surface texture - a variety of MXene film deposition techniques have been adapted. These techniques encompass vacuum-assisted filtration [11], spin-coating [12], and ink-jet printing [13]. The selection of an appropriate deposition method depends heavily on the substrate's properties and the desired characteristics of the resulting MXene film. Given the hydrophilic nature of MXenes, water serves as a suitable solvent for preparing solutions used in these various deposition methods. However, when hydrophobic substrates are employed, certain techniques, such as spin-coating, become less effective for depositing MXenes from aqueous solutions. This limitation arises because the water-based solution tends to bead up and not spread evenly on the hydrophobic surface, necessitating the incorporation of additional compounds (e.g., surfactants) to improve wetting and adhesion [12].

An alternative approach for depositing aqueous MXene solutions onto hydrophobic substrates involves ultrasonic atomization of the solution. This process generates microscopic droplets that are propelled towards the substrate under controlled pressure and flow rate. The use of a water-based solution makes the procedure environmentally friendly. As the solvent evaporates, the dispersed MXene nanoparticles are left behind, forming a layer. Due to the microscopic dimensions of the droplets, the resulting film tends to exhibit a high degree of uniformity. The small droplet size minimizes surface tension effects and promotes even distribution of the MXene material. However, this method requires heating the substrate to facilitate controlled solvent evaporation and prevent the formation of defects commonly associated with droplet-based deposition processes, such as "coffee rings" (where the solute concentrates at the droplet edge) and the Marangoni effect (which leads to fluid flow driven by surface tension gradients). The average size of the droplets generated through ultrasonic atomization is quantitatively described by the following equation [14]:

$$D = 0.34\left(\frac{8\pi\sigma}{\rho f^2}\right)^{1/3}, \tag{1}$$

where D is the mean droplet diameter, f is the frequency of the ultrasonic atomizer, ρ density of the liquid, and σ is the surface tension. As the surface tension is in relation to the viscosity of the liquids, the lower the viscosity of the atomized solution, the smaller the diameter of the droplets, under constant frequency. The aim of this paper is to establish appropriate spray deposition technology for titanium carbide thin films

with application as biosensing coatings, to study the interface processes when different metallization materials are applied on MXene film, and to test the sensor response to specific substances contained in human sweat.

2. EXPERIMENTAL SECTION

Silicon wafers coated with a thin film of silicon dioxide (SiO_2) were cleaned in acetone and used as substrates for both optimizing the spray deposition parameters and fabricating the chemoresistive sensors. The use of SiO_2-coated wafers provides a well-defined and chemically inert surface for controlled MXene film deposition. MXene films were deposited from a distilled water solution by ultrasonic atomization with SIANSONIC Ultrasonic Coating System UC330. The minimum droplet size for pure water for the used coating system is 15 μm, according to the manufacturer's specifications [15]. This value provides a benchmark for understanding the scale of the atomization process and its potential influence on film morphology. A schematic illustration of the spray deposition process, highlighting the critical parameters that govern the quality of the resulting films, is presented in Fig. 3.

Fig. 3. Simplified representation of the spray deposition process, according to Siansonic spray coater machine design

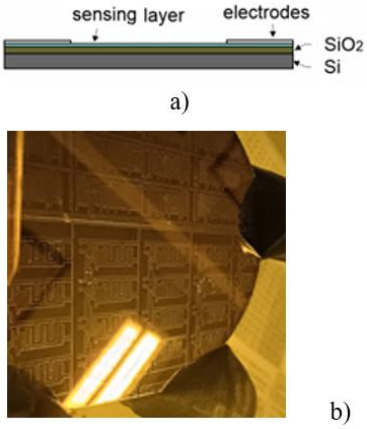

Fig. 4. Structure of the samples: a) schematic representation of cross-section of a sample; b) photograph of a fabricated silicon wafer with multiple samples

After preliminary experiments with variation of the heating plate temperature (Table 1). These initial trials were necessary to establish the ideal thermal environment for efficient film formation. The results of these preliminary experiments indicated that a substrate temperature of 130 °C was optimal, ensuring complete evaporation of the water solvent while simultaneously preventing both the sublimation of the MXene nanoparticles remaining on the surface and excessively dry conditions, where

premature evaporation leads to a powdery material with poor adhesion. Maintaining the correct temperature is a balance between promoting solvent removal and preserving the integrity of the MXene material. The subsequent parameter identified as significantly influencing film quality was the quantity of atomized solution delivered per unit time. The rate at which the MXene solution is sprayed onto the substrate directly impacts the film's thickness, uniformity, and overall structure. Therefore, the flow rate of the solution varied between 0.1 and 0.2 ml/min at constant temperature (Table 2). The number of passes of the nozzle over the substrates was chosen to be 10, so that the process of deposition is not too slow and unfit for production. The surface roughness (RMS) and topography of the Ti3C2 films, obtained at different flow rates, were estimated by atomic force microscopy (AFM) MFP-3D, Asylum Research, Oxford Instruments (Santa Barbara, CA, 93117, USA). RMS was determined with the assistance of an AFM special software – IgorPro. The topographies of the film surfaces were scanned by AFM in non-contact mode with standard silicon probes AC 140 TS. The sheet resistance of the titanium carbide films was measured by a four-point probe, FPP-5000 Veeco. Post-deposition annealing for 2 hours at 200 °C was conducted to decrease the sheet resistance and improve the MXene particle distribution. For the selected like the most uniform, highly covering the substrate and resistance stable samples, obtained at the optimal deposition conditions, titanium and aluminum contacts were produced. Titanium films were sputtered from a 3-inch titanium target in a vacuum at a base pressure of 10-6 Torr, and the sputtering argon gas pressure was 2.5x10-3 Torr at a sputtering voltage of 1 kV. The aluminum electrodes were deposited by vacuum thermal evaporation of 5N9 aluminum wire pieces at a base pressure of 10-6 Torr and evaporation current of 1 A. Schematic representation and a photograph of the fabricated structures are given in Fig. 4a and Fig. 4b, respectively. Resistance and capacitance of the interface between the metal and the sensing fills were measured by impedance analyzer Hioki IM3590 in the voltage range 0–5 V in C-V mode. The sensor response was tested by applying a microliter volume of liquids, containing MgCl2, NH3, and NaCl, with an automatic micropipette with dispenser syringe tips and measuring the current change accordingly. For this purpose, a Keithley 6485 picoammeter was used.

3. RESULTS AND DISCUSSION

In the process of establishing an appropriate spray deposition regime, it was observed that when the solution delivery rate exceeded the evaporation rate of the droplets already deposited on the substrate, an accumulation of unevaporated solvent occurred on the substrate's surface, resulting in a loss of control over the film formation process. This imbalance between delivery and evaporation hinders the creation of a well-defined film structure. Under such conditions, the force exerted by the carrier gas stream could also cause the solution to spread laterally across the substrate

surface, leading to the formation of directional streaks of material aligned with the movement of the spray head. This phenomenon compromises the film's uniformity and introduces unwanted structural artifacts. To mitigate these issues, the pressure of the carrier gas stream was reduced to 0.02 PSI, enabling controlled delivery of the atomized solution to the substrate while minimizing any significant impact on the substrate's temperature. Careful adjustment of the carrier gas pressure is essential to balance droplet transport with substrate temperature control. Subsequently, with this optimized carrier gas pressure, the solution dispensing rate was initially set to 0.2 ml/min to facilitate solvent evaporation from the substrate. This adjustment aimed to ensure sufficient time for the solvent to vaporize, preventing the accumulation of excess liquid. Prior to the annealing step, microscopic observation (not shown) revealed the presence of discrete "islands" of material, exhibiting either a lack of connectivity or only weak connections, resulting in the formation of an ultra-thin film with high electrical resistivity in those areas. The initial island-like structure reflects the limited mobility of the MXene nanoparticles and the incomplete film formation prior to thermal treatment. During the post-deposition annealing process, the MXene nanoparticles underwent migration and redistribution, facilitating their coalescence and the formation of more continuous and homogeneous layers. The application of heat provides the energy necessary for the nanoparticles to overcome surface energy barriers and coalesce into a more cohesive film. The reduction in sheet resistance served as the primary indicator of the improved film uniformity resulting from the annealing process. The inverse relationship between sheet resistance and film uniformity highlights the effectiveness of annealing in enhancing the film's structural and electrical properties.

The flow rate of the solution to be atomized was set to 0.2 ml/min, where the film showed stable and relatively low resistivity. Afterward, films with a flow rate of 0.1 ml/min and 0.15 ml/min, under constant substrate temperature, were also deposited to establish the optimal flow rate of atomized solvent and form a more uniform layer. The sheet resistances of the prepared samples were measured once more to evaluate the resulting layer uniformity. Subsequently, the surface roughness of these samples was quantified using Atomic Force Microscopy (AFM) to establish a correlation between the surface topography and the electrical resistivity of the MXene films. The flow rates, sheet resistances, and root-mean-square (RMS) roughness for the first set of investigated samples are given in Table 1. The substrate temperature, sheet resistances, and RMS for the second set of samples are presented in Table 2.

Table 1. Sheet resistance and RMS roughness of the MXene films at different temperatures

Sample №	Temperature, ^{o}C	Sheet resistance, Rs (kΩ/sq)	RMS, nm
1	120	1.95	36.38
2	130	0.26	16.16
3	140	3.32	54.47

Table 2. Sheet resistance and RMS roughness of the MXene films at different flow rates

Sample №	Flow rate, ml/min	Sheet resistance, Rs (kΩ/sq)	RMS, nm
4	0.1	0.958	26.48
5	0.15	0.156	16.96
6	0.2	2.39	34.57

The 3D AFM images of the samples 4, 5, and 6 are only given in Fig. 5a, 5b, and 5c, respectively. AFM of samples 1, 2, and 3 is not presented, as a film with reasonable quality is formed only at a temperature of 130 °C, pointed out as optimal. When the substrate temperature is too low, insufficient thermal energy impedes the adequate evaporation of the solvent, resulting in prolonged wetness of the MXene flakes. This extended wetness contributes to non-uniformity in the deposited coating as the liquid disperses unevenly. Furthermore, water molecules entrapped within the film structure can induce hydrolysis reactions, inhibiting proper film consolidation and accelerating oxidation processes over time, effects that may not be directly observable via AFM. Conversely, excessively high substrate temperatures promote rapid solvent evaporation, precluding the MXene flakes from adequately settling and aligning into an ordered structure. This rapid desiccation leads to immediate and uncontrolled stacking of the MXene flakes, resulting in the formation of dense, thick layers characterized by substantial gaps between the individual flakes. This uncontrolled deposition can promote the development of macroscopic defects such as large pores and even structural ruptures within the film. These observations align consistently with findings reported in previous research [16, 17]. As can be seen, the lower the RMS roughness is, the lower the sheet resistance of the samples is, which also confirms that the optimal flow rate of delivered solution to the substrate was 0.15 ml/min.

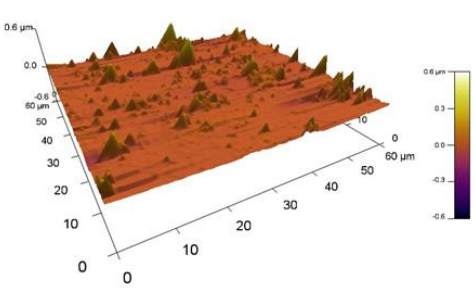

a) (Fig. 5)

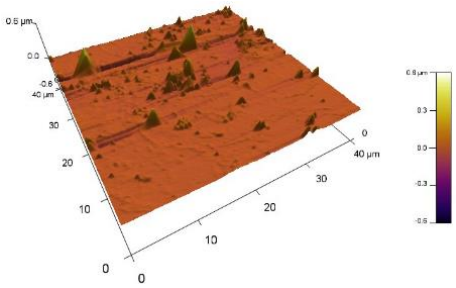

b) (Fig. 5)

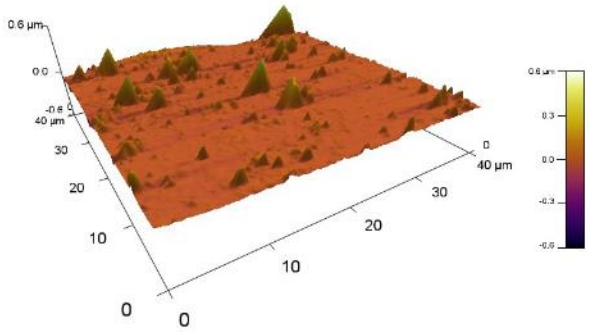

c)

Fig. 5. 3D AFM images of a) Sample 4; b) Sample 5 and c) Sample 6

Chemoresistive sensor structures were fabricated by depositing titanium (Ti) and aluminum (Al) metal contacts onto the MXene films that exhibited the lowest measured sheet resistance. Selecting the lowest interface (contact) resistance films ensures that the inherent conductivity of the MXene layer is maximized, optimizing the sensitivity of the overall sensor device. Titanium was strategically selected as one of the contact materials based on the theoretical prediction that it would establish an Ohmic contact with the MXene sensing layer. An Ohmic contact is characterized by a linear current-voltage relationship, indicating minimal contact resistance and unimpeded charge flow between the metal and the semiconductor. This expectation stemmed from the fact that MXenes are titanium-containing materials, suggesting a potential for favorable interfacial bonding and minimal Schottky barrier formation. The similar chemical composition aims to minimize energy barriers at the interface.

Conversely, aluminum was intentionally chosen to form a contact that would induce a charge carrier barrier, creating a depletion layer within the titanium carbide, thereby forming a Schottky contact. A Schottky contact exhibits a non-linear current-voltage characteristic due to the presence of a potential barrier at the metal-semiconductor interface. The energy level alignment at the interface for the titanium metallization case is depicted in Fig. 6.

Energy level diagrams help to visualize the relative positions of the Fermi levels and work functions of the materials, providing insights into charge transport mechanisms. When an Ohmic contact is formed, and the work functions of the contacting materials (MXene and Ti in this case) are sufficiently close, a depletion layer of significant width to impede charge transfer across the contact interface does not develop. The absence of a substantial depletion layer allows for efficient and linear charge injection and extraction, minimizing contact resistance.

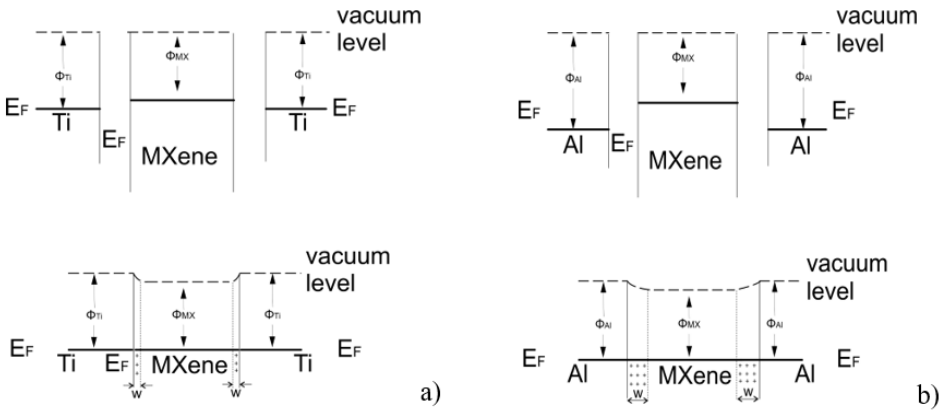

Fig. 6. Energy levels of the structure: a) before contacting the MXenes with titanium electrodes and after contacting and creating an Ohmic contact; b) before contacting the MXenes with aluminum electrodes and after contacting and creating a Schottky contact. Φ_{Ti}, Φ_{Al} and Φ_{MX} are work functions of titanium, aluminum, and MXene, respectively

The work function of MXenes after annealing at 200 °C is reported to be approximately 4.2 eV [18], while the work function of titanium is approximately 4.33 eV. These values, while not identical, are sufficiently close to suggest that an Ohmic contact formation is achievable. The formation of Ohmic and Schottky contacts for titanium and aluminum metallizations, respectively, was experimentally confirmed through capacitance-voltage (C-V) and resistance-voltage (R-V) measurements. C-V and R-V techniques are standard methods for characterizing the electrical behavior of metal-semiconductor junctions. In these measurements, the contact capacitance and resistance were evaluated as a function of the applied bias voltage, providing information about the presence and nature of interfacial barriers. These measurements are shown in Fig. 7. The bias voltage effectively modulates the width of the depletion region, influencing the capacitance and resistance of the junction.

As evidenced in Fig. 7b, the contact resistance for the aluminum contacts exhibits a distinct drop at approximately 1.1 V, and the corresponding capacitance curve displays an inflection point. The inflection point marks the voltage at which the built-in potential of the Schottky barrier is overcome, leading to a significant increase in current flow.

These observations are indicative of the presence of a contact barrier that is surmounted at this voltage, leading to increased current conduction and a subsequent sharp decrease in resistance. In contrast, Fig.7a demonstrates that the characteristics for the titanium contacts are predominantly linear, exhibiting only minor variations around an average resistance value, a behavior that is typical for an Ohmic contact where little or no interface barrier exists. The linear behavior suggests that the resistance is relatively constant across the applied voltage range, indicative of unimpeded charge transport. Based on the absence of an inflection point in the C-V curves

for the titanium contacts (Fig. 7a), it can be inferred that there is a lack of a significant depletion region and an absence of band bending in the energy band diagram of the materials near the interface. This supports the conclusion that an Ohmic contact is indeed formed between titanium and the MXene layer, without requiring a specific "turn-on" voltage to overcome an interfacial barrier. This is desirable for sensor applications as the response will ideally be linear and sensitive across the entire operating voltage range.

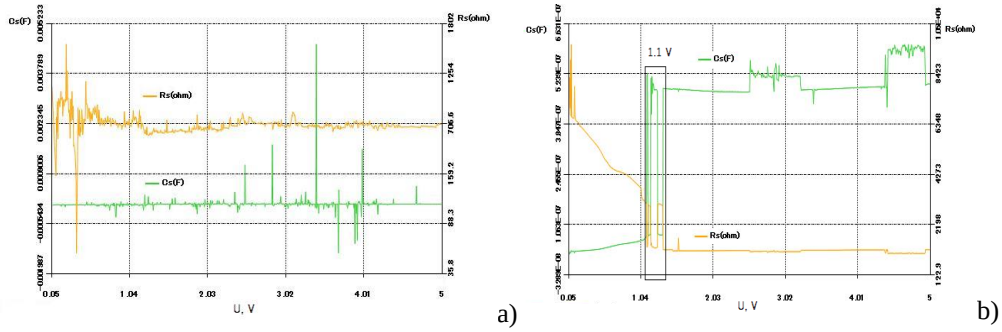

a) b)

Fig. 7. C-V graphs of a) Ti/MXene contacts and b) Al/MXene contacts

$MgCl_2$, NH_3, and NaCl are compounds found in the sweat, and their concentrations depend on individual factors such as age, sex, race, and health status. For a clinically healthy middle-aged person, typical values of these parameters range within, for example, 0.02-0.2 mg/mL for $MgCl_2$, 1-3 μg/mL for NH_3, and 1-3 mg/mL for NaCl [19]. Solutions of $MgCl_2$, NH_3, and NaCl were prepared with concentrations in these ranges and were drop-casted on the MXene sensing layers using a laboratory micropipette with a minimum dose of 10 μL. To investigate the sensors' sensitivities toward the different compounds and their dependence on the liquid volume, the current through the structure was measured under constant voltage, and an increasing number of droplets was placed over the titanium carbide. The current through the chemoresistive sensor with Ti metallization, under the influence of these compounds separately, is shown in Fig. 8. The sensor with Ti contacts was the most responsive toward $MgCl_2$, where the change in conductivity follows the change in the concentration of the substance with distinct current values The response time was 1 s and after removing the influence of the solution the recovery time was found to be 15 s for low volumes in the range of 10-30 μL and 28 s for higher volumes. Lower sensitivity can be observed towards NH_3, and no sensitivity towards NaCl. The current through the chemoresistive sensor with Al metallization, under the influence of the different compounds separately, is shown in Fig. 9.

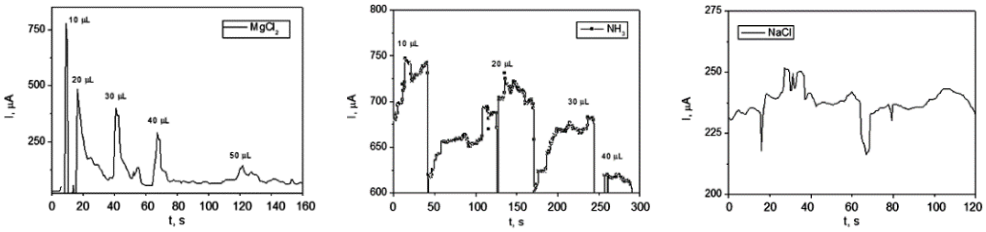

Fig. 8. Sensor's response with Ti_3C_2/Ti interface towards a) $MgCl_2$, b) NH_3, and c) NaCl [20]. Reprinted with permission from IEEE – R. Tomov et al., Investigation of Spray-Coated Titanium Carbide MXene Thin Films and Their Application in Biosensors, in: Proc. XXXIII International Scientific Conference Electronics - ET2024, September 17-19, 2024.

The response of the structure with Al contacts was longer until a stable signal was measured, and it was weaker as compared to the sensor structure with Ti contacts (mean current of 500 μA compared to 750 μA for the structure with Ti contacts). Also, the sensors with Al metallization have lower sensitivity; a measurable response was observed for amounts of substances above 20 μL (in contrast to the titanium electrode, where this value is 10 μL), which can be ascribed to the contact barrier formation between the Al electrodes and the MXene.

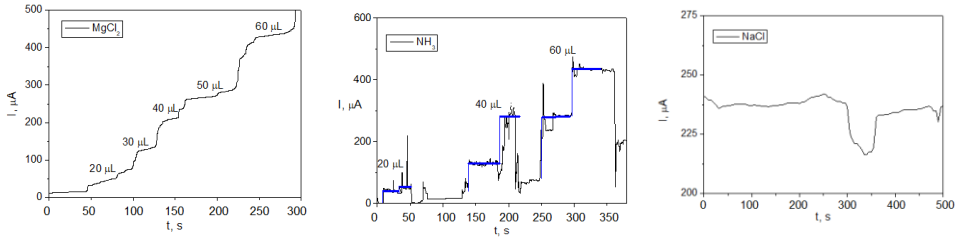

Fig. 9. Sensor's response with Ti_3C_2/Al interface towards a) $MgCl_2$, b) NH_3, and c) NaCl [20]. Reprinted with permission from IEEE – R. Tomov et al., Investigation of Spray-Coated Titanium Carbide MXene Thin Films and Their Application in Biosensors, in: Proc. XXXIII International Scientific Conference Electronics - ET2024, September 17-19, 2024.

Figure 10 a-c displays the response characteristics of the fabricated sensors when exposed to step changes (both increments and decrements) in the concentrations of the target analytes: magnesium chloride ($MgCl_2$), ammonia (NH_3), and sodium chloride (NaCl). This type of analysis, known as dynamic response testing, allows us to evaluate the sensor's real-time behavior, including its sensitivity, response time, and recovery time, and assess its ability to track changes in analyte concentration. It's

essential to evaluate the suitability of the sensor for continuous monitoring applications. For the needs of the present experiment, a chemoresistive measurement principle is the most suitable solution, which is the reason to select the case with the Ohmic contact formed between Ti electrode and the MXene sensitive coating. A lag can be observed in each of the plots, where the sensor doesn't respond instantaneously to the concentration change. Additionally, a gradual saturation occurs as the concentration reaches the maximum value. This is due to the time it takes for the analyte to interact with the sensor and the sensor to reach its maximum detection capability.

Most reasonable variations in the sensor signal (current) corresponding to changes in $MgCl_2$ concentration can be noted in Fig. 10a. Upon initial exposure to $MgCl_2$, a rapid and pronounced change in current is observed, indicating a high sensitivity and a fast response time. The lack of dissociation of the compound into Mg^{2+} and $2Cl^-$ ions each likely contributes to reduced charge transfer at the surface, leading to a significant decrease in the device's conductivity. The nearly linear response to increasing $MgCl_2$ concentrations implies the sensor's suitability for quantitative measurement across a broad concentration range, which is typical in the sweat composition. In contrast, the sensor's response to NH_3 (Fig. 10b) is less pronounced and more gradual compared to $MgCl_2$, with a slower response time. This can be attributed to the slower diffusion of ammonia molecules into the MXene interlayer spaces or slower reaction kinetics between their surface functional groups. It may involve electron acceptor behavior, decreasing the conductivity of the MXene film.

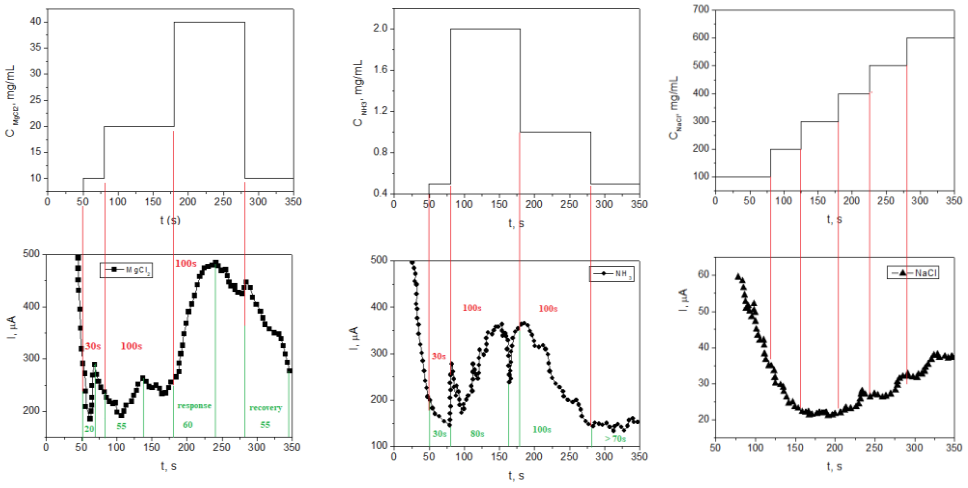

a) b) c)

Fig. 10. Response characteristics of the sensors at step change (increment and decrement) in the corresponding analyte's concentration: a) for $MgCl_2$ component; b) for NH_3 component; c) for NaCl component.

While a clear decrease in current is observed with increasing NH_3 concentration, the less distinct steps and smaller magnitude of the response compared to $MgCl_2$ suggest a lower sensitivity and less reliable quantification of NH_3 using this sensor configuration. The sensor's reaction to NaCl is minimal and relatively noisy, confirming a poor sensitivity to this analyte (Fig. 10c). This indicates a very weak interaction between Na^+ and Cl^- ions and the MXene surface. The absence of a significant change in conductivity suggests that the surface functional groups of the MXene are less reactive towards these particular ions or that a specific activation energy is required for adsorption to occur. The nature of the MXene functionalization is important to consider when talking about the binding to each specification.

The response time can be seen in the same graphs as the time from the addition of the new concentration until the sensor shows a stable signal. The response time varied depending on the analyte and its concentration. The recovery time refers to the time from when the analyte concentration is reduced (or removed) until the sensor's signal returns to its baseline or initial value. Recovery time can be seen at the end of the curves and can also be affected by factors such as the analyte's properties and the sensor material. For the $MgCl_2$ sensor, the time response increased slightly with the concentration increase, starting from 20 s for the lowest concentration and reaching 60 s at the highest concentration of 40 mg/mL, with a recovery time of 55 s after saturation. For the NH_3 sensor, the response time for the lowest concentration was 30 s and reached 80 s for the highest concentration of 2 mg/mL. Afterwards, although the concentration was further decreased, the strong saturation of the sensor resulted in even higher response time of 100 s and recovery time of more than 70 s, without a clear trend of restoring the initial condition of the sensor. For the NaCl, the sensor structure cannot exhibit differentiated response and recovery times.

4. CONCLUSIONS

In summary, this study successfully optimized a technology for depositing titanium carbide MXene films from an aqueous solution utilizing ultrasonic atomization. By carefully controlling parameters such as substrate temperature, solution flow rate, and carrier gas pressure, uniform and conductive MXene films were achieved. Leveraging these optimized films, chemoresistive sensor architectures were fabricated, incorporating both titanium (Ti) and aluminum (Al) contacts to strategically exploit their distinct interfacial properties. The selection of Ti was based on its ability to form an Ohmic contact with the MXene sensing layer, facilitating efficient charge injection and extraction, while Al was chosen for its potential to create a Schottky barrier, enhancing sensitivity through modulation of the depletion region. The sensing capabilities of these structures were then evaluated toward key sweat components. The resulting sensors exhibited a distinct response profile, demonstrating the highest sen-

sitivity towards $MgCl_2$, a moderate response to NH_3, and a minimal, unstable response to NaCl. The observed differences in sensitivity are likely attributed to variations in the strength of interaction and charge transfer efficiency between each analyte and the MXene surface functional groups, in addition to the influence of the contact material on charge transport at the MXene-metal interface - a relationship that warrants further investigation. These initial findings suggest that the developed sensing structures hold promise for the detection, and potentially the quantification, of specific biomarkers in sweat, thereby contributing to the advancement of non-invasive health monitoring strategies.

However, it is crucial to acknowledge existing limitations and future directions. Further research is necessary to address the sensor's cross-sensitivity to other sweat components or environmental factors, like changes in temperature and humidity, and to fully elucidate the complex mechanisms governing analyte-MXene interactions. Specifically, future studies should focus on: (1) investigating the sensor's response to complex mixtures of sweat analytes to assess its performance in more realistic scenarios; (2) characterizing the influence of environmental variables, such as temperature and humidity, on the sensor's stability and sensitivity; (3) exploring the long-term stability and aging characteristics of the MXene films and sensor devices under prolonged exposure to relevant environmental conditions. Ultimately, the goal is to engineer robust, selective, and reliable MXene-based sensors for continuous and non-invasive monitoring of human health, which necessitates a comprehensive understanding of the factors influencing their performance and stability over time.

5. ACKNOWLEDGMENT

Funding is partially under the program for support of Ph.D. students at the Technical University of Sofia – NIS (R&D sector), Grant № 232ПД0015-03 for the consumables supplied, and partially under the program of the European Union-NextGenerationEU through the National Recovery and Resilience Plan of the Republic of Bulgaria, project № BG-RRP-2.004-0005 for the ultrasonic spray coater. Research equipment of Distributed Research Infrastructure INFRAMAT, part of the Bulgarian National Roadmap for Research Infrastructures, supported by the Bulgarian Ministry of Education and Science, was used in this AFM investigation.

REFERENCES

[1] Z. ZHANG ET AL., Sweat as a Source of Non-Invasive Biomarkers for Clinical Diagnosis: An Overview (2024) *Talanta*, **273**, 125865, online https://doi.org/10.1016/j.talanta.2024.125865.

[2] S. PATLE AND D. ROTAKE, Recent Advances, Technological Challenges and Requirements to Predict the Future Trends in Wearable Sweat Sensors: A Critical Review (2024) *Microchem J*, **200**, 110457, online: https://doi.org/10.1016/j.microc.2024.110457.
[3] C. F. CONSOLAZIO, L. O. MATOUSH, R. A. NELSON AND ET. AL., Excretion of Sodium, Potassium, Magnesium and Iron in Human Sweat and the Relation of Each to Balance and Requirements(1963) *J Nutr*, **79** (4), 407–415, online: https://doi.org/10.1093/jn/79.4.407.
[4] M. SALEH, A. GUL, A. NASIR AND ET. AL., Comprehensive Review of Carbon-Based Nanostructures: Properties, Synthesis, Characterization, and Cross-Disciplinary Applications (2024) *J. Ind. Eng. Chem*, **146**, 176-212, online: https://doi.org/10.1016/j.jiec.2024.11.052.
[5] A. JAHANGIRI-MANESH AND ET AL., Molecularly Imprinted Polymer-Based Chemiresistive Sensor for Detection of Nonanal as a Cancer-Related Biomarker (2022) *Microchem J*, **173**, 106988, online: https://doi.org/10.1016/j.microc.2021.106988.
[6] B. CHETTRI, A. THAPA, S. K. DAS AND ET. AL., First Principle Insight Into Co-Doped MoS2 for Sensing NH3 and CH4 (2022) *Facta Universitatis*, **35**, 43–59, online: https://doi.org/10.2298/FUEE2201043C.
[7] S. SARKAR ET AL., *Surfaces and Interfaces* (2024), **51**, 104628.
[8] N. CHEN, W. YANG AND C. ZHANG, *STAM* (2021), **22** (1), 917–930.
[9] online: https://www.cheaptubes.com/product/mxene-ti3c2-materials/?srsltid=AfmBOopusHdfbX780W9Ip05Y1ZSTM0icU97A1mZlNsq8N2JBTKd-XmLT.
[10] R. K. CHOUDHURY, B. BHAGAT, K. MALI, R. POKAR AND A. DASHORA, *Appl. Surf. Sci* (2022), **603**, 154426.
[11] Z. ZHANG AND ET AL., (2021) *Nano Energy*, **88,** 106257, online: https://doi.org/10.1016/j.nanoen.2021.106257.
[12] M. ZHANG ET AL., *Ceram. Int.* (2019), **45** (15), 19467–19472.
[13] G. WANG, R. ZHANG, H. ZHANG AND K. CHENG, *J Colloid Interface Sci* (2023), **645**, 359–370.
[14] R. J. LANG, Ultrasonic Atomization of Liquids (1962) *J. Acoust. Soc. Am*, **34**, 6–8, online: https://doi.org/10.1121/1.1909020.
[15] Ultrasonic Atomization (2022), online: https://www.siansonic.com/technology-ultrasonic-atomization.
[16] T. GUO AND ET AL., *ACS Nano* (2023), **17** (4), 3737-3749, online: https://doi.org/10.1021/acsnano.2c11180.
[17] R. RAHMATI, M. SALARI, M. ASHOURI-SANJANI AND ET AL., (2024) *Small*, **20**, 2308320, online: https://doi.org/10.1002/smll.202308320.
[18] T. SCHULTZ, N.C. FREY, K. HANTANASIRISAKUL, S. PARK, S. J. MAY, V. B. SHENOY, Y. GOGOTSI, AND N. KOCH, *Chem. Mater*. (2019), **31**, 6590–6597.
[19] L. BAKER, Physiology of Sweat Gland Function: The Roles of Sweating and Sweat Composition in Human Health (2019) *Temperature (Austin)*, **6** (3) 211–259, online: https://doi.org/10.1080/23328940.2019.1632145.
[20] R. TOMOV, V. STRIJKOVA, V. KATROVA AND M. ALEKSANDROVA, in: Proc. XXXIII International Scientific Conference Electronics - ET2024, 17-19 September 2024.

Received October 4, 2025